Research Article | Vol. 28, No. 26 / 21 December 2020 / Optics Express 39387
Optics EXPRESS

Curvature sensing using a hybrid polycarbonate-silica multicore fiber

TOMMY BOILARD,[1,*] GUILLAUME BILODEAU,[1] STEEVE MORENCY,[1] YOUNÈS MESSADDEQ,[1] RICHARD FORTIER,[2] FRANÇOIS TRÉPANIER,[3] AND MARTIN BERNIER[1]

[1]Center for Optics, Photonics, and Lasers (COPL), Université Laval, Québec (QC) G1V 0A6, Canada
[2]Center for Northern Studies (CEN), Université Laval, Québec (QC) G1V 0A6, Canada
[3]TeraXion Inc., Québec (QC) G1P 4S8, Canada
[*]tommy.boilard.1@ulaval.ca

Abstract: We report on the development of a novel hybrid glass-polymer multicore fiber integrating three 80 µm polyimide-coated silica fibers inside a 750 µm polycarbonate cladding. By inscribing an array of distributed FBGs along each segment of silica fiber prior to the hybrid fiber drawing, we demonstrate a curvature sensor with an unprecedented precision of 296 pm/m^{-1} around 1550 nm, about 7 times more sensitive than sensors based on standard 125 µm multicore fibers. As predicted by theory, we show experimentally that the measured curvature is insensitive to temperature and strain. Also, a more precise equation to describe the curvature on a simple bending setup is presented. This new hybrid multicore fiber technology has the potential to be extended over several kilometers and can find high-end applications in 3D shape sensing and structural health monitoring.

1. Introduction

Quasi-distributed sensors based on fiber Bragg grating (FBG) written in standard optical fibers are gaining popularity for remote sensing of physical parameters, such as strain and temperature, because of their small size, their immunity to electromagnetic interference, their resistance to harsh environment, their high mechanical strength as well as their ease to be distributed over long distance [1]. FBGs have been used in a variety of applications to measure temperature from cryogenic temperature [2] up to 1000 °C [3] and in radioactive environment [4], strain with extremely high resolution [5], pressure [6], refractive index [7] and chemical [8], to cite only a few. Standard optical fibers have the drawback of being unable to measure bending, which is of interest for numerous applications, such as 3D shape sensing [9] and structural health monitoring [10]. To overcome this limitation, two options are generally used.

The first one is the inscription of FBGs in multicore fibers or eccentric core fibers, where the cores that are not in the center will feel strain or compression depending on the amplitude of the bending and its direction. Flockhart et al. were the first to show the possibility to measure bending in both axis using UV-written FBGs in a 4-core optical fiber [11]. Even if their FBGs didn't have the same reflectivity and shape due to the UV inscription, their demonstration was quite promising. Recently, Barrera et al. have shown similar results with the same type of fiber, but with an array of 15 distributed FBGs written in all four cores of the fiber, for a total length of 58 mm [12]. Butov et al. have shown a thirtyfold increase in sensitivity by using a 2.1 mm silica rod with 4 cores located near the edge [13]. However, the writing of FBGs in multicore fibers is always a challenge, since the individual writing in each core of the fiber is difficult, the interrogation of multicore fiber requires a complex fanout photonic component, the fiber coating needs to be remove for UV exposure, thus reducing the strength of the fibers, and none of these demonstrations are distributed over more than 50 cm. So far, to our knowledge, only Bronnikov et al. have demonstrated the direct writing of arrays of FBGs throught the polyimide coating of a

#411363 https://doi.org/10.1364/OE.411363
Journal © 2020 Received 6 Oct 2020; revised 27 Nov 2020; accepted 5 Dec 2020; published 14 Dec 2020

Optics EXPRESS

multicore fiber in each of its cores using the fs plane-by-plane writing technique with satisfactory results [14]. However, although the writing of robust FBGs was reported using the femtosecond phase-mask writing technique [15], it is yet to be demonstrated with the plane-by-plane writing technique. Other techniques, not based on FBGs, successfully demonstrated curvature sensing in multicore fibers. For example, distributed curvature sensing has been demonstrated in a multicore fiber based on Brillouin scattering [16]. Compared to FBGs, Brillouin-based sensors have the advantages of being continuously distributed with the capacity of monitoring strain and temperature over several kilometers. However, this comes with the drawback of a reduced spatial resolution and less precise measurement of the physical parameters, compared to distributed FBGs. Another demonstration shows that a Michelson interferometer can be made by combining the output of a dual-core fiber, thus precisely measuring the relative phase between the two cores [17]. However, given the nature of this technique, curvature sensing cannot be distributed over long fiber lengths. Overall, the use of multicore fibers as distributed shape sensors is still very limited.

The second option to measure bending is to fix a standard optical fiber on an assembly that transfer the bending to the fiber as strain. It is generally done by fixing the FBG on a cantilever beam. Lu et al. used this idea to measure water flow based on the bending of a cantilever beam upon which a FBG was fixed [18]. However, theses demonstrations generally increase the size of the sensors considerably, which are often comparable to their electrical counterparts. Other ways of transfering the bending also exist. For example, Roesthuis et al. glued three fibers with 4 FBGs in each of them inside three grooves made into a flexible nitinol needle, in order to precisely reconstruct the shape of the needle inside soft tissue [19]. Moon et al. have made a hybrid epoxy-silica multicore fiber by epoxy-molding three separated single-core fibers with FBGs pre-written in them [20]. The sensor is less than 900 µm in diameter and its length is 11.5 cm, which is ultimately limited by the proposed assembly method. However, the use of a polymer as a structural element instead of silica increases the sensor sensitivity to external perturbation, due to of its lower rigidity and it overcomes the complications of writing FBGs in multicore fibers.

Based on this idea, we proposed a novel assembly method for a hybrid polymer-silica multicore fiber in which three standard 80 µm polyimide-coated with distributed arrays of FBGs pre-written in them are assembled inside a microstructured polycarbonate preform, the latter being drawn on a draw tower. Limited by the available fiber, the sensor is 55 m-long, has a diameter of 750 µm and, due to the spacing between each fiber, has a sensitivity of 296 pm/m^{-1}, which is 7 times higher than a standard multicore fiber. It is also shown that the measured curvature (and its direction) is insensitive to strain and temperature, up to 0.35 % and 120 °C, respectively. Since the proposed assembly method is based on the drawing of a preform, its size and geometry can be easily changed and its length is ultimately limited by the size of the preform and the length of the fibers available, thus having the potential to be drawn over several kilometers.

2. Principle of operations

A uniform FBG is a periodic modulation of the refractive index of the core of an optical fiber. This periodic modulation creates constructive interference for a backward propagating mode at a precise wavelength, named the Bragg wavelength. It is calculated as

$$\lambda = 2n_{\text{eff}}\Lambda \tag{1}$$

where λ is the Bragg wavelength, n_{eff} is the effective refractive index of the mode in the fiber and Λ is the period of the grating. For most standard silica fibers, the value of n_{eff} is about 1.448 at 1550 nm. When the grating is written with the phase-mask writing technique, $\Lambda = \Lambda_m/2$, where Λ_m is the period of the phase-mask. This means that the Bragg wavelength is fixed by the period of the phase-mask. Once written, the Bragg wavelength is highly dependent on external perturbations, such as strain, temperature and bending, since these perturbations change the

Optics EXPRESS

period of the grating and its effective refractive index. The relative change in wavelength $\Delta\lambda/\lambda$ can be expressed as

$$\frac{\Delta\lambda}{\lambda} = (1 - P_e)\,\epsilon + \left(\alpha + \frac{1}{n_{\text{eff}}}\frac{dn_{\text{eff}}}{dT}\right)\Delta T + (1 - P_e)\,r\cos(\theta + \phi)\kappa \tag{2}$$

where the first term is the effect of external strain (ϵ), the second term is the effect of a temperature change (ΔT) and the third term is the effect of curvature ($\kappa = 1/R$, where R is the radius of curvature of the fiber at this location), which is non-zero only for cores that are off-center ($r \neq 0$). In this equation, P_e is the strain-optic coefficient, α is the effective coefficient of thermal expansion, dn_{eff}/dT is the thermo-optics coefficient, r is the distance from the center of the fiber (or more generally the distance from the neutral axis) to the center of the core, θ is the angle between the axis of bending and the axis made from the center of the fiber to the core 1 (chosen for convenience) and ϕ is the angle between the core in consideration and the core 1. Fig. (1) shows a sketch of a multicore fiber with a curvature κ at an angle θ. Standard values for P_e (0.22) and dn_{eff}/dT (1.1×10^{-5} °C^{-1}) in silica fibers are found in the literature [21]. The effective coefficient of thermal expansion, α, for an assembly of two materials, can be approximated with [22] :

$$\alpha = \alpha_{\text{SiO2}} + (1 - P_e)\,(\alpha_{\text{PC}} - \alpha_{\text{SiO2}})\,\frac{A_{\text{PC}}E_{\text{PC}}}{A_{\text{SiO2}}E_{\text{SiO2}} + A_{\text{PC}}E_{\text{PC}}} \tag{3}$$

where α_{SiO2} and α_{PC} are the coefficients of thermal expansion of silica and polycarbonate, and A and E are the area and the Young modulus of both materials, respectively. This equation means that a composite fiber made from silica and polycarbonate will expands proportionally to α_{SiO2}, as usual, but it will also be pulled (thus the $(1 - P_e)$ term) by an amount of $\alpha_{\text{PC}} - \alpha_{\text{SiO2}}$, weighted by the relative stiffness of both materials.

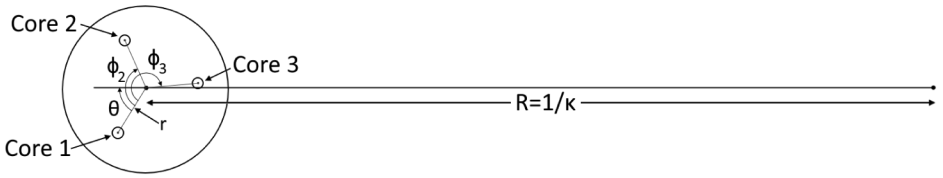

Fig. 1. Definition of θ and ϕ according to the direction of the curvature κ.

According to Eq. (2), the change in wavelength for two cores in a multicore fiber is the same in strain and temperature, however they will be different in curvature since their sensitivities depend on ϕ. It is convenient to define the differential mesure between two Bragg wavelengths, $\delta\lambda_{ij}$, to get rid of the external strain/temperature [23]. It is defined as

$$\delta\lambda_{ij} = \frac{\Delta\lambda_i}{\lambda_i} - \frac{\Delta\lambda_j}{\lambda_j} = (1 - P_e)\cdot\left(r_i\cos(\theta + \phi_i) - r_j\cos(\theta + \phi_j)\right)\kappa \tag{4}$$

Assuming that 3 cores of a n-cores multicore fiber can respect the condition $r_1 = r_2 = r_3 = r$ and $\phi_1 = 0°$, $\phi_2 = 120°$, $\phi_3 = 240°$ (valid for most 3-cores and 7-cores fibers), two simple equations can be obtained for both κ and θ :

$$\kappa = \frac{1}{(1 - P_e)\cdot 3r}\sqrt{(\delta\lambda_{12} + \delta\lambda_{13})^2 + \left(\sqrt{3}\delta\lambda_{32}\right)^2} \tag{5}$$

$$\theta = \arctan\left(\frac{\sqrt{3}\delta\lambda_{32}}{\delta\lambda_{12} + \delta\lambda_{13}}\right) \tag{6}$$

Optics EXPRESS

Moreover, with the same conditions as above, it is easily shown that

$$\frac{\Delta\lambda_1}{\lambda_1} + \frac{\Delta\lambda_2}{\lambda_2} + \frac{\Delta\lambda_3}{\lambda_3} = 3\left((1 - P_e)\,\epsilon + \left(\alpha + \frac{1}{n_{\text{eff}}}\frac{dn_{\text{eff}}}{dT}\right)\Delta T\right) \tag{7}$$

Therfore, the summation of the 3 relative changes in wavelength is equal to the external perturbation on the fiber (strain/temperature) and doesn't depend on the curvature of the fiber. Only three cores are needed for a full description of the perturbation on the fiber, meaning that a central core, insensitive to bending, is not needed. It is important to note that strain and temperature, as is almost always the case for simple sensors made from FBGs, can't be discriminated from one another.

3. FBG writing setup

The arrays of FBGs, pre-written in the silica fibers before drawing the polycarbonate preform, were fabricated in house at COPL using the femtosecond scanning phase mask writing technique, on a setup similar to the one described in [24]. This technique has the advantage of not degrading the mechanical strength of the fiber [15]. The 35 fs pulses, centered at 806 nm, are generated at 1 kHz by a regenerative amplifier (Astrella, Coherent). The gaussian pulses (11 mm at $1/e^2$) are truncated into approximately rectangular pulses of 11mm × 500 µm by a slit, then tightly focused by an acylindrical lens (f = 8 mm) through an ebeam phase mask with 20 different 6 mm-long uniform periods along its length (Λ_1 = 1045 nm, Λ_{20} = 1090 nm), to the core of the fiber through its protective polyimide coating. The lens, mounted on piezoelectric actuators, allows the beam to be scanned over the entire core's cross section, increasing the overlap between the FBG and the mode propagating in the fiber core, thus increasing the FBG's reflectivity. This is required given that the material's interaction of femtosecond pulses with such a short focusing lens leads to an inscription width of only about 0.8 micron [24], significantly smaller than the 4.2 µm fiber core diameter. The beam can also be translated along the length of the fiber (and the phase mask) by a linear air bearing translation stage, which gives flexibility on the length of the grating. This translation, in combination with the 20 periods ebeam phase mask, is also used to select the period of the grating. To unroll the fiber and write FBGs at precise predetermined locations along the fiber, a winder and an unwinder are installed on both side of the FBGs writing setup.

The fiber used in this experiment is a 80 µm polyimide-coated fiber (SM1500(4.1/80)P, Fibercore), due to its small size, its higher confinement (characterized by smaller bending losses), and its polyimide coating, needed for the polycarbonate drawing at high temperature (180 °C). To increase its photosensitivity, the fiber was deuterium-loaded at 2000 psi for 2 weeks at room temperature prior to writing. This treatment is optional, but it reduces the risk of damaging the coating of the 80 µm fiber during trans-jacket inscription since it lowers the energy needed for inscription, while making it much faster. Due to fiber availability (200 m), the FBGs were written in three sections of 65 m. Using the winding setup, the first 25 m of each fiber was left blank, since it was expected that the size of the hybrid multicore fiber during drawing would vary at the beginning before reaching equilibrium and it would be discarded. A dense array of ten 4 mm-long FBGs were written at this position in each fiber. Each fiber was then moved by 5 m, then FBGs were written at each meter for 10 m. The rest of the fibers afterward were left blank. The three fibers containing the arrays of FBGs were then thermally annealed at 120 °C for 24 h to stabilize them and to remove the residual deuterium. The reflectivity spectrum of an array of FBGs written in one of the fiber, measured with a commercial FBGs interrogator (si155, Micron Optics), is presented in Fig. 2(a), and the position of the FBGs along the length of the fiber is presented in Fig. 2(b).

Optics EXPRESS

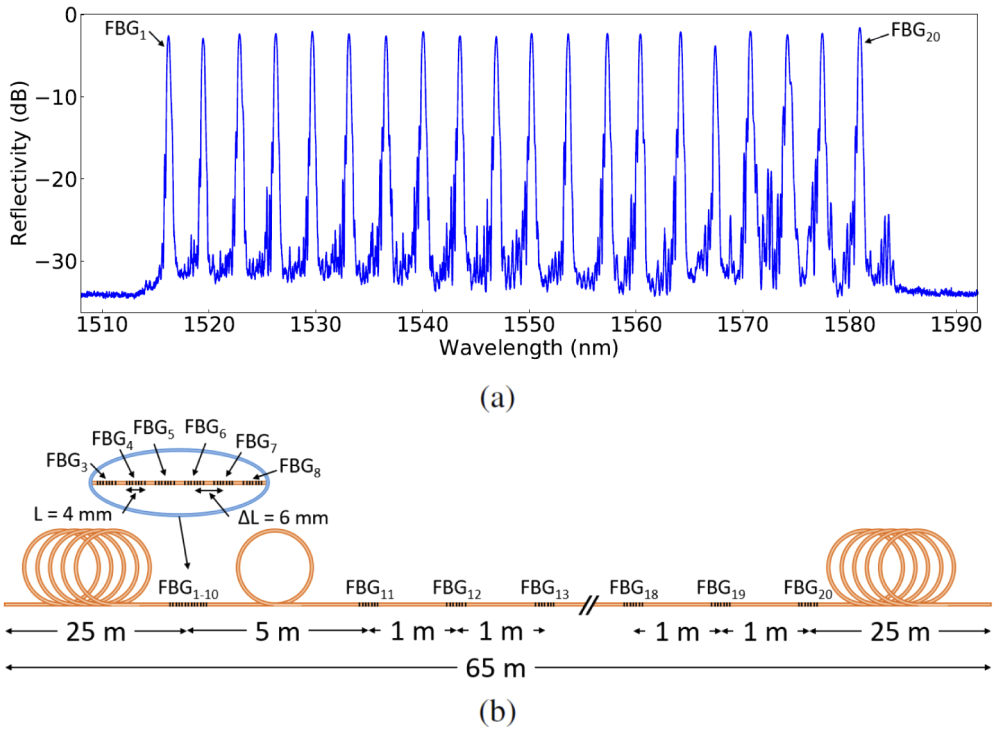

Fig. 2. (a) Reflectivity spectrum of an array of FBGs in one of the 80 µm polyimide-coated fiber and (b) position of the FBGs along its length.

4. Results

4.1. Hybrid glass-polymer multicore fiber assembly and drawing

The hybrid glass-polymer multicore fiber was drawn from a polycarbonate preform made with the stack and draw method. Polycarbonate was chosen as cladding material given its large Young modulus (2.3 GPa) as well as its excellent chemical stability. Its design, shown in Fig. 3(a), starts with a polycarbonate hollow-cylinder (OD : 25.4 mm, ID : 19.05 mm). Three polycarbonate capillaries (OD : 8.8 mm, ID : 3 mm) are inserted inside it, with their outer diameter chosen such that they fit perflecty inside the polycarbonate hollow-cylinder (it can be shown, by simple geometry, that $d = (2\sqrt{3} - 3)D$, where d and D are the diameters of the inner and outer circle, respectively). This assures that they are at 120° from each other. Three other capillaries (OD : 3 mm, ID : 0.6 mm) are inserted inside the others in order to reduce their inner diameter. The remaining voids between the capillaries and the outer hollow-cylinder are partially filled with polycarbonate rods of varying size. One end of the preform is heated until all the rods and capillaries are combined together, assuring that all parts are fixed and that the three capillaries are closed, making the initial positionning of the fibers much easier. The assembled polycarbonate preform before drawing is shown in Fig. 3(b).

The polycarbonate preform was drawn in house on a custom made drawing tower, designed for soft-glass and plastic fibers. The three 80 µm polyimide-coated fibers with arrays of FBGs pre-written in them are inserted inside each of the three capillaries of the preform through the preform, until the closed end. The polycarbonate's transparency and the orange tint of the polyimide-coated silica fibers made it easy to see whether or not the fibers are at the same position inside the preform. To feed the polyimide-coated fiber during drawing, a 3-arms spool holder was

Optics EXPRESS

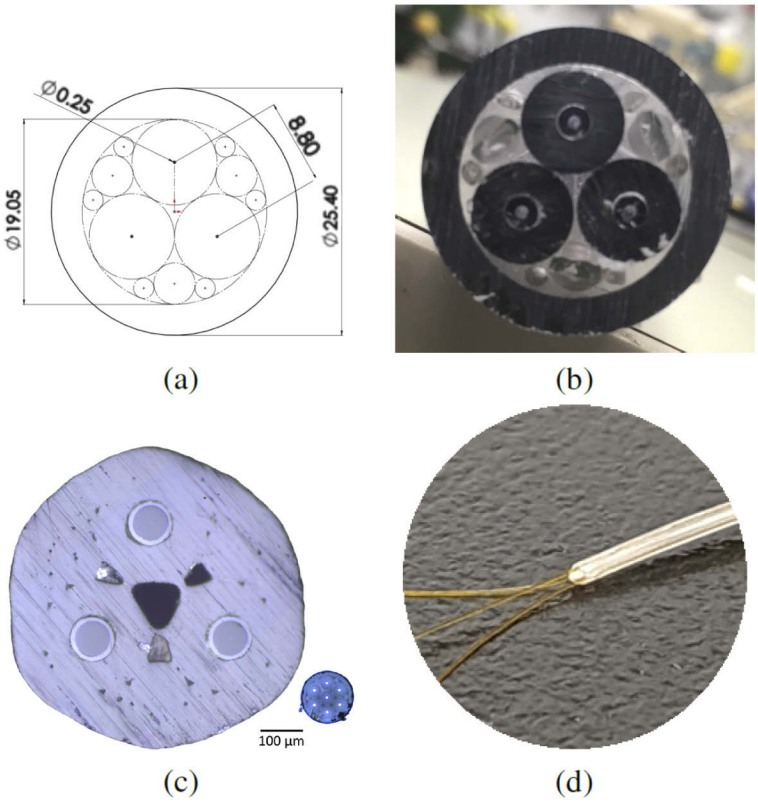

Fig. 3. (a) Initial design of the preform, (b) assembled polycarbonate preform prior to drawing, (c) cross-section of the hybrid multicore fiber after drawing and (d) the three polyimide-coated fibers coming out of the polycarbonate. For size comparaison, the cross-section of an uncoated standard multicore fiber (SM-7C1500(6.1/125), Fibercore) is shown in (c).

designed, 3D-printed, and fixed over the top of the preform to hold the three spools containing the fibers. The preform is heated at 180 °C and drawn at a speed of 1 m/min. The speed and the temperature were slightly corrected until a measured constant diameter of 750 µm was obtained. The first 10 m of the resulting hybrid multicore fiber were discarded since its size was varying in this section.

Due to the limited availability of the polyimide-coated silica fiber, the result of the drawing is a 55 m-long hybrid polycarbonate-silica multicore fiber with ten dense sensing points at 15 m (since the first 10 m were discarded), and then another ten sensing points at 1 m interval, starting at 20 m. A cross-section of a polished end of the fiber was observed on a standard optical microscope and is shown in Fig. 3(c). For size comparison, a cross-section of a 125 µm uncoated standard multicore fiber (SM-7C1500(6.1/125), Fibercore) is also shown in Fig. 3(c). With its coating, the fiber is twice this size (245 µm), meaning the hybrid multicore fiber is only three times bigger than a standard 125 µm silica fiber. The diagonal lines in the polycarbonate are results from the polishing, while the triangle in the center and the ones between each fiber are hollow. They were present in the preform and did not collapsed on themselves. However, the voids in the preform that were nearer to the outside did collapsed, and they are still slightly visible as black dots in the polycarbonate, delimiting the different capillaries and rods. Since the voids in the center did not collapsed on themselves while the voids near the outside did, it is safe to assume that this is due

Optics EXPRESS

temperature gradient from the outside (hotter) to the inside (colder). It could be overcome by increasing the temperature slightly and better filling the void in the preform. The outside of the hybrid polycarbonate-silica multicore fiber is hexagonal instead of round, as it can sometimes be seen on silica microstructured fibers. Again, this could have been overcome by filling the preform better near the capillaries, since there are two voids on both side of each capillaries that have collapsed and have brought the outside closer to the center, explaining the six flats. The cores, claddings and coatings of the three 80 µm fibers are seen at roughly 120° from each other (122.9°, 121.0° and 116.1°, starting from the top and going clockwise) and at a distance of approximately 180 µm from the center (176 µm, 188 µm and 172 µm, starting from the top and going clockwise). The deviation can be explained by the initial diameters of the polycarbonate rods and capillaries, which have variations that are bigger than what is generally observed with silica material. Also, some errors of positioning can occur during the collapse of the preform during drawing. In addition, the outline of the polyimide-coated fibers in the cross-section are not perfect circle (especially the top one), meaning the polishing has probably moved the real position of the fiber and distorted the polycarbonate near the fiber by forcing the fiber into it. It should be noted that the cross-section of the hybrid fiber presented in Fig. 3(c) was measured near the beginning of the drawn fiber, a few meters before the dense array of 10 FBGs. We didn't cut the fiber along its length to preserve its integrity for future experiments. The geometry uniformity along the fiber length has therefore not been precisely characterized and will be the subject of further studies.

To connectorized the hybrid multicore fiber, patch cords need to be spliced to the three fibers inside it. To do so, the hybrid multicore fiber is first cut at the desired position using standard mechanical fiber stripper, then the end of the fiber is dipped in liquid dichloromethane for a few minutes. The polycarbonate is easily wiped off from the three polyimide-coated fibers, insensitive to dichloromethane [25]. A picture of the end of the fiber where the three polyimide-coated fibers are seen coming out of the polycarbonate fiber is shown in Fig. 3(d). The tip of these fibers are then uncoated, cleaved and spliced to standard fiber patch cords. This method is really robust since the polyimide coating of the fibers remain unaffected from its contact with dichloromethane.

4.2. Curvature sensitivity

The setup used to characterize the sensitivity of multicore fibers is made of two fiber clamps, initially at a distance L, one stationary and the other mounted on a micrometric screw, which can be brought closer by an amount ΔL. The fiber, due to its small diameter compare to its length, will buckle instead of compressing. The angle of the bending can also be forced, without changing the bending amplitude nor the shape of the fiber, by a rotating mount, located at $L/2$, on which a fork-like beam is attached. In order to compare the sensitivity of the hybrid multicore fiber to a standard multicore fiber (SM-7C1500(6.1/125), Fibercore), dense arrays of ten 4 mm-long FBGs, spaced 6 mm from each others (center to center), were written through its coating in 3 lateral cores of its 7 cores, using the same FBGs writing setup as described earlier. The Bragg wavelength of each FBGs are monitored using a commercial FBGs interrogator (si155, Micron Optics), with a wavelength accuracy of 1 pm.

In the litterature, it is common to assume that the shape of the fiber in this setup will follow an arc of a circle, giving a constant bending κ along the fiber, obtained by resolving the following transcendent equation [26] :

$$\sin\left(\frac{L\kappa}{2}\right) = \frac{(L-\Delta L)\kappa}{2} \tag{8}$$

However, after measuring the change in wavelength of an array of FBGs in a multicore fiber on this setup, it became clear that the assumptions made to derive Eq. (8), and Eq. (8) itself, are not valid. To overcome this issue, using Euler-Bernoulli beam theory, a set of equations was developed to described the deflection of the fiber more precisely than the arc of a circle approximation. The details on the development of these equations are found in Supplement 1 of

Optics EXPRESS

this article. The main result is that the bending κ is not constant along the length of the fiber, and even change sign, being negative for about the first and last quarter of the fiber. It is expressed as

$$\kappa(x) = \frac{2a(6x^2 - 6Dx + D^2)}{\left[1 + (2ax(x-D)(2x-D))^2\right]^{3/2}} \approx 2a(6x^2 - 6Dx + D^2) \tag{9}$$

where $D = L - \Delta L$ and the parameter a is obtained by calculating the curve length of the deflection of the fiber, $y = ax^2(x-D)^2$. However, the integral cannot be solve analytically. By solving it numerically, the result can be fitted and a can be approximated with good agreement by

$$a \approx \frac{11.7}{D^3}\left(\frac{\Delta L}{D}\right)^{0.541} \tag{10}$$

To compare Eq. (8) and Eq. (9), the FBGs array on the standard multicore fiber was positionned on the bending setup with an initial length of $L = 99$ mm, and one of the fiber clamp was moved closer by $\Delta L = 2$ mm. The calculated deflection of the fiber based on Eq. (8) (in black) and Eq. (9) (in blue) are provided in Fig. 4(a). The main visible difference between the two curves is near the edges, where the fibers are clamped. Since the fibers are clamped, they are forced to be horizontal at $x = 0$ and $x = D$, which is not the case for the curve in black. Near the center of the fiber ($x \sim D/2$), both equations seem to follow approximately the same trend in term of deflection and change in deflection. This can lead to the erroneous conclusion that the shape of the fiber can be approximated by an arc of a circle near the center. The curvature κ calculated from Eq. (8) (in black) and Eq. (9) (in blue), and the one calculated from Eq. (5) using the measured Bragg wavelength of the 10 FBGs in the standard multicore fiber, using $P_e = 0.22$ and $r = 35\mu$m, are shown in Fig. 4(b). It is important to stress that no fit was done in any of the equations to obtain these curves, and the sensitivity of the standard multicore fiber ($\Delta\lambda/\Delta\kappa$) is $(1 - P_e)r\lambda = 42.3$ pm/m^{-1} near 1550 nm. The figure shows clearly that approximating the shape of the fiber by an arc of a circle (black curve) leads to a constant curvature along the fiber, plus a underestimated value of around 2.4 for the curvature at the center of the fiber (nearly independant of L and ΔL), leading to a suposely 2.4 times more sensitive sensor. Meanwhile, Eq. (9) seems to be in good agreement with the measured value, both in the center and closer to the edge, even accounting for the change in the direction of κ near $D/4$ and $3D/4$.

With Eq. (9) in hand, the hybrid multicore fiber is characterized on the same setup. On the green plane in Fig. 5(a) lies the relative wavelength changes of each core of the fiber for different curvatures applied, at an arbitrary angle. The core 3 (black dots) is in extension (positive change in wavelength), the core 2 (blue dots) is in contraction (negative change in wavelength), while the core 1 (red dots) is almost constant and near zero, meaning it lies close to the neutral axis. This allows for a rapid estimation that $\theta \approx 90°$. In fact, the signs and amplitudes of the wavelength changes of each core can be used to assess rapidly the angle of curvature with a precision of $\pm 15°$. Equation (5) and Eq. (6) are used to fit the lines in the figure. To get good agreements, the values used in the equations are $r = 245\mu$m and $\theta = 96°$. This value for r is higher than the one measured on the cross-section of Fig. 3(c) ($r = 180\mu$m), but its important to note that the cross-section of the hybrid multicore fiber was taken at one end of the 55 m-long fiber in order to keep the entire fiber in one piece. The cross-section at the middle of the fiber, where the measurement took place, is smaller. Noting that the curvature depends on $r\cos\theta$, another axis, denoted $\Delta\lambda/\lambda_{sin}$, can be added on the figure, such as

$$\left(\frac{\Delta\lambda}{\lambda_{cos}}\right)^2 + \left(\frac{\Delta\lambda}{\lambda_{sin}}\right)^2 = ((1 - P_e)\, r\kappa)^2 \tag{11}$$

which is used to draw a cone (shown in gray in the figure). This means that for each curvature κ, one can draw a circle of radius $(1 - P_e)r\kappa$ on which the three points $(\Delta\lambda/\lambda_{cos}, \Delta\lambda/\lambda_{sin})$ must lied

Optics EXPRESS

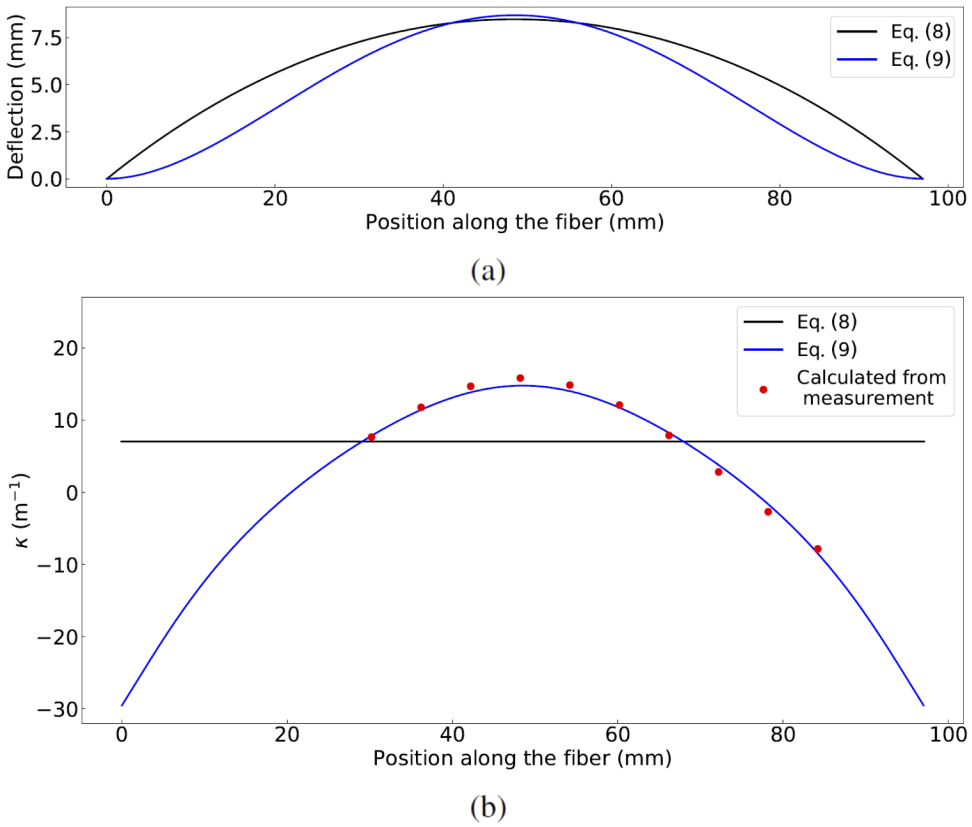

Fig. 4. Calculated (a) fiber deflection and (b) curvature from Eq. (8) and Eq. (9). The red dots in (b) are calculated from the wavelength measurement using Eq. (5).

(shown with in solid square in the figure), at $\theta = 120°$ from each other. The measured relative changes in wavelength are a projection on the green plane of these three points. The effect of curvature and rotation is a translation of the solid squares along the κ axis onto the cone and a rotation of the solid squares around the κ axis (onto a constant radius circle), respectively, thus changing the projection on the green plane. The characterization gives a sensitivity to curvature of 296 pm/m^{-1} near 1550 nm, which is 7 times greater than the standard silica multicore fiber (42.3 pm/m^{-1} shown previously). This is expected since the cores are about 7 times more distant from the center. Figure 5(b) shows the relative change in Bragg wavelength for each core according to the angle of the bending, normalized such that the cores have a maximum at approximately 0°, 120° and 240°. Equation (2) is fitted on each data set using the same r as above. The measurements follow roughly a cosine curve, with the deviations being attributed to the bending setup. This conclusion is supported by the fact that the same deviations were present during the standard multicore fiber characterization, which is known to be perfectly circular.

The sensitivity of the hybrid multicore fiber to strain and temperature was also compared to the standard multicore fiber. They were both characterized on a standard FBG characterization bench. For temperature characterization, the fibers were put individually inside a fiber oven and the temperature was increased by steps of 10 °C from room temperature (20 °C) up to 70 °C. Fig. 6(a) shows the result of this characterization. The sensitivity of the standard multicore fiber is close to the expected value for a silica fiber. For the hybrid multicore fiber, this sensitivity has been characterized to be 3.8 times larger than the standard fiber, which is due to the higher

Optics EXPRESS

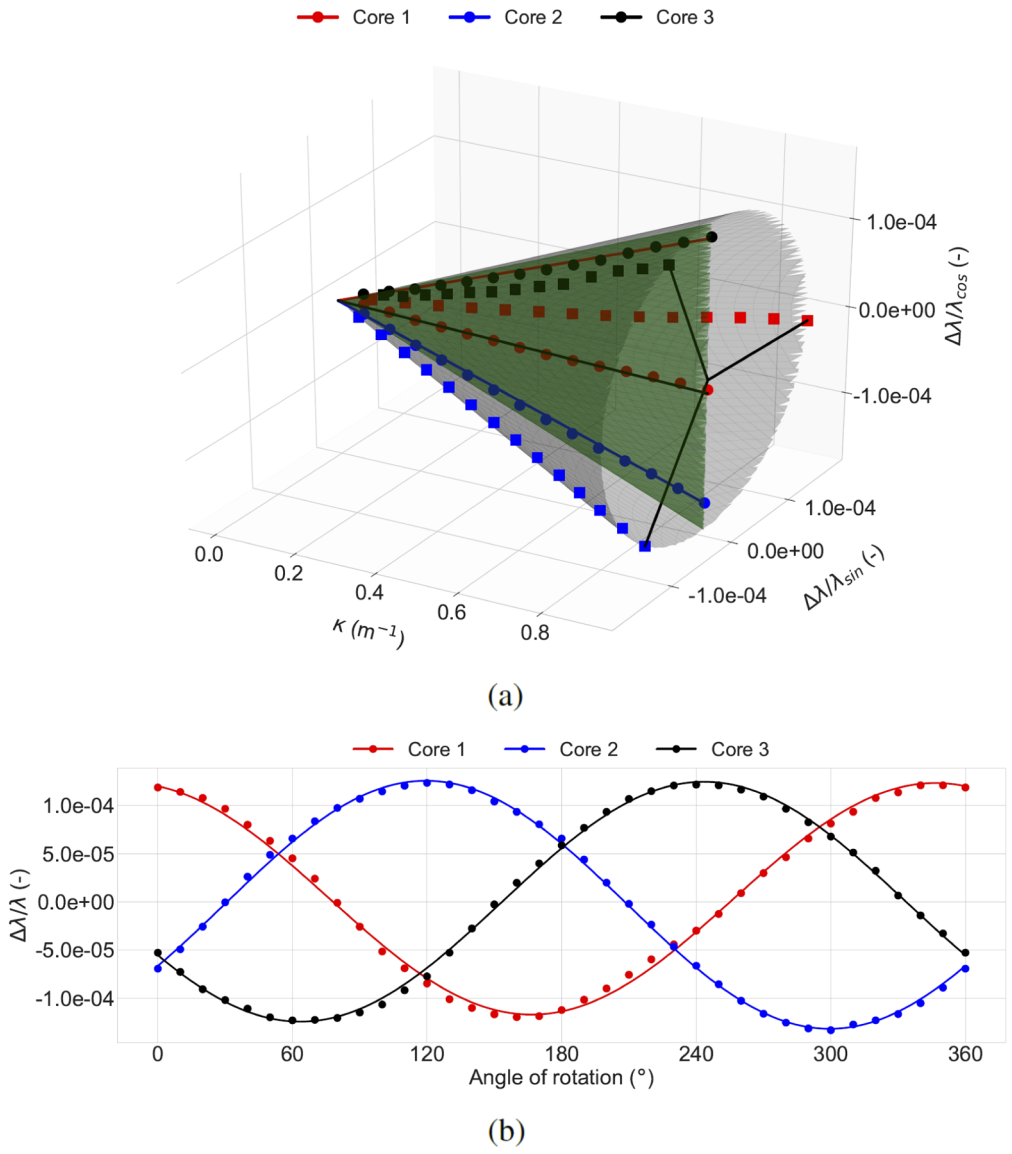

Fig. 5. Relative change in wavelength of the three cores of the hybrid multicore fiber for (a) different curvatures (κ) and (b) different angles. In (a), the measured relative wavelength changes, shown as solid circles, are located on the green plane, while the solid squares lie on a 3D cone of radius $(1 - P_e)r\kappa$ and are at 120° from each other. The relative wavelength changes, in solid circles, can be view as a projection of the solid squares onto the green plane, and the effect of curvature and rotation is a translation of the solid squares along the κ axis onto the cone and a rotation of the solid squares around the κ axis (onto a constant radius circle), respectively.

Optics EXPRESS

coefficient of thermal expansion of the polycarbonate serving as a cladding. Using Eq. (3) with the values of α_{PC} and E_{PC} given by the manufacturer, the main contribution of the temperature sensitivity of this hybrid fiber is its thermal expansion, $\alpha = 24.6 \times 10^{-6} °C^{-1}$. Taking into account the change in refractive index, this gives a theoretical sensitivity of $\Delta\lambda/\lambda = 32.1 \times 10^{-6}\Delta T$, which is in pretty good agreement with the measured value ($\lambda/\lambda = 29.1 \times 10^{-6}\Delta T$). Fig. 6(b) shows the result of the characterization of both fibers in strain. While they are both in the same order of magnitude, the hybrid multicore fiber has a slightly larger sensitivity (+11%) than that of the standard multicore fiber.

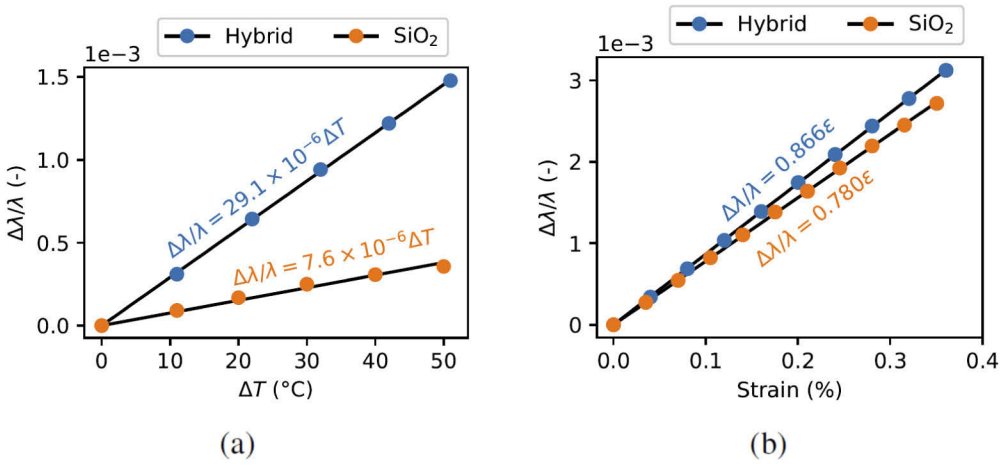

Fig. 6. Comparison of the sensitivity of both multicore fibers to (a) a change in temperature and (b) strain.

Moreover, the validity of Eq. (4), which states that the differential measurement between the relative wavelength change of two different cores of a multicore fiber is insensitive to temperature and strain, was tested using the measured wavelength changes from the temperature and strain characterizations presented in Fig. 6. Fig. 7(a) shows the differential measurement between two cores of the standard multicore fiber, $\delta\lambda_{ij}$, versus the change in temperature. Similar results were obtained for the hybrid multicore fiber. Comparing the magnitude of wavelength changes for the relative change in wavelength and the differential measurement for the characterization in temperature, it is seen that the differential measure is approximately zero (it is in average 400 to 800 times less than the relative changes in wavelength), meaning the effet of temperature change is close to being totally suppressed. In Fig. 7(b), the same characterization was done, but according to strain. This time, the differential measure between two cores is now, in average, 8000 times less than the relative changes in wavelength.

Finally, the maximum curvature that could be measured with the hybrid multicore fiber was estimated by measuring the minimal radius of curvature before the polycarbonate suffers from plastic deformation. This was done by applying a known radius of curvature of decreasing size on the fiber for 10 s, then letting the fiber free. Below a radius of curvature of $R = 1.25$ cm ($\kappa = 80\ m^{-1}$), the fiber suffers from plastic deformation. This represents the maximum curvature that could be sensed while keeping the physical integrity of the sensor. On the other hand, given the limited spectral spacing of 3.4 nm between each FBG (determined by the distributed phase-mask configuration used, see section 3) and the large curvature sensitivity of 296 pm/m^{-1}, a local curvature above 11.5 m^{-1} (R below 8.7 cm) will result in a spectral overlap between adjacent FBGs. Half of this value is expected for a curvature that locally changes in direction, such as a S-shape curve. These values represent the maximum curvature that can be sens with the actual sensor configuration. Given that the interrogator has a significantly larger spectral

Optics EXPRESS

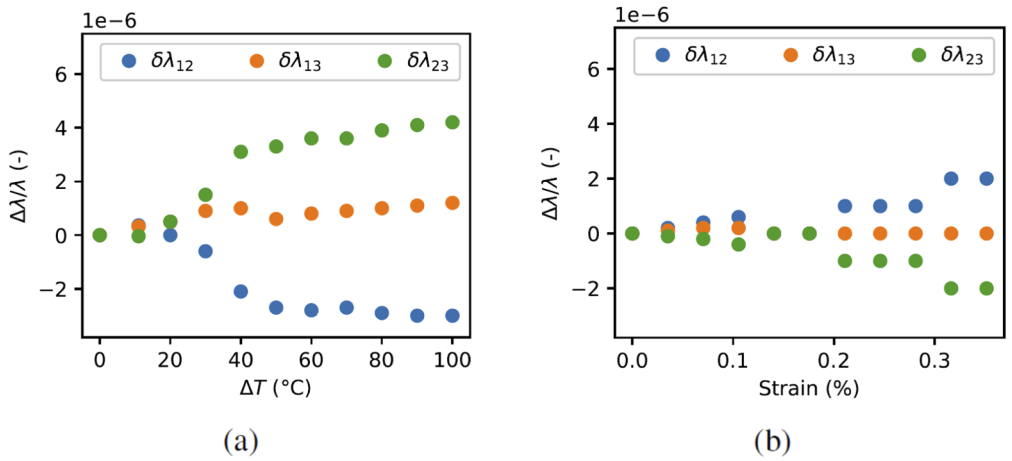

Fig. 7. Differential measure between the cores for (a) temperature change and (b) strain.

range compared to the FBG array (160 nm vs 35 nm for the dense distributed array), such limits could be easily increased by using a distributed phase-mask with a larger pitch spacing.

5. Conclusion

A novel 55 m-long hybrid polycarbonate-silica multicore fiber drawn from a microstructured polycarbonate preform has been presented. The assembly, with an outside diameter of 750 µm, integrates three standard 80 µm polyimide-coated fiber in which arrays of FBGs were pre-written prior to drawing. The sensitivity of this sensor, in good agreement with the theory, is of 296 pm/m^{-1} around 1550 nm, 7 times higher than sensors based on FBGs written in standard 125 µm multicore fibers. The hybrid multicore fiber also has several advantages over traditionnal multicore fiber, such as easier connectivity and easier writing of FBGs. This hybrid multicore fiber technology has the potential to be extended over several kilometers, and can find applications for distributed 3D shape sensing and structural health monitoring.

Funding

Natural Sciences and Engineering Research Council of Canada (CRDPJ-543631-19); Canada Foundation for Innovation; Fonds de recherche du Québec – Nature et technologies; Canada First Research Excellence Fund.

Acknowledgments

The authors thank Stéphan Gagnon and Myriam Blanchet for helpful discussions and technical assistance. This research was supported by the Sentinel North program of Université Laval, made possible, in part, thanks to funding from the Canada First Research Excellence Fund.

Disclosures

The authors declare no conflicts of interest.

See Supplement 1 for supporting content.

Optics EXPRESS

References

1. A. D. Kersey, M. A. Davis, H. J. Patrick, M. LeBlanc, K. P. Koo, C. G. Askins, M. A. Putnam, and E. J. Friebele, "Fiber grating sensors," J. Lightwave Technol. **15**(8), 1442–1463 (1997).
2. C. Lupi, F. Felli, A. Brotzu, M. A. Caponero, and A. Paolozzi, "Improving fbg sensor sensitivity at cryogenic temperature by metal coating," IEEE Sens. J. **8**(7), 1299–1304 (2008).
3. D. Grobnic, C. W. Smelser, S. J. Mihailov, and R. B. Walker, "Long-term thermal stability tests at 1000°c of silica fibre bragg gratings made with ultrafast laser radiation," Meas. Sci. Technol. **17**(5), 1009–1013 (2006).
4. G. Laffont, R. Cotillard, N. Roussel, R. Desmarchelier, and S. Rougeault, "Temperature resistant fiber bragg gratings for on-line and structural health monitoring of the next-generation of nuclear reactors," Sensors **18**(6), 1791 (2018).
5. G. Skolianos, A. Arora, M. Bernier, and M. J. F. Digonnet, "Slow light in fiber bragg gratings and its applications," J. Phys. D: Appl. Phys. **49**(46), 463001 (2016).
6. M. G. Xu, L. Reekie, Y. T. Chow, and J. P. Dakin, "Optical in-fibre grating high pressure sensor," Electron. Lett. **29**(4), 398–399 (1993).
7. W. Liang, Y. Huang, Y. Xu, R. K. Lee, and A. Yariv, "Highly sensitive fiber bragg grating refractive index sensors," Appl. Phys. Lett. **86**(15), 151122 (2005).
8. S. Silva, L. Coelho, J. M. Almeida, O. Frazao, J. L. Santos, F. X. Malcata, M. Becker, M. Rothhardt, and H. Bartelt, "H_2 sensing based on a pd-coated tapered-fbg fabricated by duv femtosecond laser technique," IEEE Photonics Technol. Lett. **25**(4), 401–403 (2013).
9. P. Wilkening, F. Alambeigi, R. J. Murphy, R. H. Taylor, and M. Armand, "Development and experimental evaluation of concurrent control of a robotic arm and continuum manipulator for osteolytic lesion treatment," IEEE Robot. Autom. Lett. **2**(3), 1625–1631 (2017).
10. M. Majumder, T. K. Gangopadhyay, A. K. Chakraborty, K. Dasgupta, and D. K. Bhattacharya, "Fibre bragg gratings in structural health monitoring—present status and applications," Sens. Actuators, A **147**(1), 150–164 (2008).
11. G. M. H. Flockhart, W. N. MacPherson, J. S. Barton, J. D. C. Jones, L. Zhang, and I. Bennion, "Two-axis bend measurement with bragg gratings in multicore optical fiber," Opt. Lett. **28**(6), 387–389 (2003).
12. D. Barrera, I. Gasulla, and S. Sales, "Multipoint two-dimensional curvature optical fiber sensor based on a nontwisted homogeneous four-core fiber," J. Lightwave Technol. **33**(12), 2445–2450 (2015).
13. O. V. Butov, A. P. Bazakutsa, Y. K. Chamorovskiy, A. N. Fedorov, and I. A. Shevtsov, "All-fiber highly sensitive bragg grating bend sensor," Sensors **19**(19), 4228 (2019).
14. K. Bronnikov, A. Wolf, S. Yakushin, A. Dostovalov, O. Egorova, S. Zhuravlev, S. Semjonov, S. Wabnitz, and S. Babin, "Durable shape sensor based on fbg array inscribed in polyimide-coated multicore optical fiber," Opt. Express **27**(26), 38421–38434 (2019).
15. M. Bernier, F. Trépanier, J. Carrier, and R. Vallée, "High mechanical strength fiber bragg gratings made with infrared femtosecond pulses and a phase mask," Opt. Lett. **39**(12), 3646–3649 (2014).
16. Z. Zhao, M. A. Soto, M. Tang, and L. Thévenaz, "Distributed shape sensing using brillouin scattering in multi-core fibers," Opt. Express **24**(22), 25211–25223 (2016).
17. L. Yuan, J. Yang, Z. Liu, and J. Sun, "In-fiber integrated michelson interferometer," Opt. Lett. **31**(18), 2692–2694 (2006).
18. P. Lu and Q. Chen, "Fiber bragg grating sensor for simultaneous measurement of flow rate and direction," Meas. Sci. Technol. **19**(12), 125302–125309 (2008).
19. R. J. Roesthuis, M. Kemp, J. J. van den Dobbelsteen, and S. Misra, "Three-dimensional needle shape reconstruction using an array of fiber bragg grating sensors," IEEE/ASME Trans. Mechatron. **19**(4), 1115–1126 (2014).
20. H. Moon, J. Jeong, S. Kang, K. Kim, Y. Song, and J. Kim, "Fiber-bragg-grating-based ultrathin shape sensors displaying single-channel sweeping for minimally invasive surgery," Opt. Lasers Eng. **59**, 50–55 (2014).
21. R. Kashyap, "Fabrication of bragg gratings," in *Fiber Bragg Gratings* (Academic, 2009).
22. S. Sridhar, S. Sebastian, and S. Asokan, "Temperature sensor based on multi-layer mos_2 coated etched fiber bragg grating," Appl. Opt. **58**(3), 535–539 (2019).
23. M. J. Gander, W. N. MacPherson, R. McBride, J. D. C. Jones, L. Zhang, I. Bennion, P. M. Blanchard, J. G. Burnett, and A. H. Greenaway, "Bend measurement using bragg gratings in multicore fibre," Electron. Lett. **36**(2), 120–121 (2000).
24. J. Habel, T. Boilard, J.-S. Frenière, F. Trépanier, and M. Bernier, "Femtosecond fbg written through the coating for sensing applications," Sensors **17**(11), 2519 (2017).
25. DuPont, DUPONT™ KAPTON® summary of properties, https://www.dupont.com/content/dam/dupont/amer/us/en/products/ei-transformation/documents/DEC-Kapton-summary-of-properties.pdf.
26. H. Zhang, Z. Wu, P. P. Shum, R. Wang, X. Q. Dinh, S. Fu, W. Tong, and M. Tang, "Fiber bragg gratings in heterogeneous multicore fiber for directional bending sensing," J. Opt. **18**(8), 085705 (2016).